Journal of The Electrochemical Society, **156** (1) H52-H58 (2009)
0013-4651/2008/156(1)/H52/7/$23.00 © The Electrochemical Society

Metallorganic Chemical Vapor Deposition of ZnO Nanowires from Zinc Acetylacetonate and Oxygen

Jason B. Baxter[a,z] **and Eray S. Aydil**[b]

[a]*Department of Chemical and Biological Engineering, Drexel University, Philadelphia, Pennsylvania 19104, USA*
[b]*Department of Chemical Engineering and Materials Science, University of Minnesota, Minneapolis, Minnesota 55455, USA*

ZnO nanowires were grown by metallorganic chemical vapor deposition from zinc acetylacetonate hydrate and oxygen without using any seed particles or templates. Nanowires grew epitaxially on sapphire substrates to form dense arrays but with random orientation on F:SnO_2 and glass. Nanowire morphology was studied as a function of deposition conditions, including substrate temperature, zinc partial pressure, and growth duration. Water evolves from the initially hydrated precursor during the first 30 min of growth, resulting in deposition of a thin polycrystalline film. The grains of this film then act as nucleation sites for nanowire growth from the now-anhydrous precursor. After several hours of growth, the precursor decomposes to ZnO, resulting in nucleation of smaller secondary nanowires on the sides of the first nanowires. These branched structures with high surface area may have potential applications in dye-sensitized solar cells and sensors. Transmission electron microscopy shows that the nanowires are crystalline, and photoluminescence is nearly free of defect emissions.
 [DOI: 10.1149/1.3006390]

Manuscript submitted May 22, 2008; revised manuscript received September 18, 2008. Published November 7, 2008.

ZnO nanowires have received much attention recently because of their potential applications in dye-sensitized solar cells,[1-4] sensors,[5-7] UV lasers,[8,9] and field emitters.[10-12] Controlling semiconductor morphology and microstructure is critical to these applications. ZnO nanowire arrays have been grown by several methods, including metallorganic chemical vapor deposition (MOCVD),[3,13-18] thermal evaporation,[19-28] electrodeposition,[29-34] and chemical bath deposition.[4,35-38] These growth methods often require separate steps to seed the substrate with metal catalyst,[19,22,27,39-41] ZnO nanoparticles,[4,36] or films.[42,43] Another approach is to template the growth with anodic alumina membranes.[30,34,44,45]

MOCVD offers several advantages compared to other growth methods. MOCVD typically demands lower temperatures than thermal evaporation, provides higher purity materials than solution methods, and is compatible with current semiconductor processing technology. Diethyl zinc[16] and zinc acetylacetonate[13-15] [$Zn(acac)_2$] are two of the most commonly used zinc sources for MOCVD growth of ZnO nanowires. Chemical vapor deposition (CVD) using $Zn(acac)_2$ has yielded different morphologies, ranging from polycrystalline thin films[46-49] to micron-diameter whiskers[50] to sub-100 nm nanowires.[13,15] The morphology depends on the substrate temperature, deposition chamber pressure, and oxygen source. Transparent, conductive polycrystalline ZnO films have been grown with H_2O or H_2O_2 rather than with O_2.[46] Whiskers with diameters on the order of microns have been grown by atmospheric pressure MOCVD,[50] while low-pressure MOCVD presented herein yields thinner nanowires. In this article, we present the growth of ~100 nm diameter ZnO nanowires from $Zn(acac)_2$ and oxygen. We show that the morphology and orientation of the nanowires depend on the substrate material, substrate temperature, pressure, and temperature history of the precursor. By examining the evolution of the precursor over time, we have correlated the three sequential stages of ZnO growth (nucleation of a polycrystalline film, primary nanowire growth, and growth of branching secondary nanowires) to the three states the precursor undergoes during heating [$Zn(acac)_2$ hydrate, anhydrous $Zn(acac)_2$, and ZnO]. By replacing the spent precursor during the growth, we have grown ZnO nanowires with a dendritic branched structure with large surface areas. Photoluminescence (PL), transmission electron microscopy (TEM), and X-ray photoelectron spectroscopy (XPS) indicate that the nanowires are crystalline with low defect concentrations.

[z] E-mail: jbaxter@drexel.edu

Experimental

ZnO nanowires were grown by MOCVD from $Zn(acac)_2$ hydrate [$Zn(C_5H_7O_2)_2 \cdot xH_2O$, also known as zinc pentanedionate] and oxygen on various substrates, including fluorine-doped tin oxide, silicon, glass and *a*- or *c*-plane sapphire. $Zn(acac)_2$ is a white powder at room temperature and has a reported melting point of 137°C, but this melting point can vary substantially depending on its degree of hydration. $Zn(acac)_2$ was purchased from Aldrich and used as received. $Zn(acac)_2$ vapor was generated by heating $Zn(acac)_2$ to temperatures in the range of 75–125°C and fed into the MOCVD chamber by flowing Ar carrier gas over the powder. In this temperature range, the precursor either dehydrates, melts, and then evaporates, or it sublimes directly. The temperature history of the $Zn(acac)_2$ powder affects its degree of hydration and morphology, which in turn affect $Zn(acac)_2$ and H_2O partial pressures in the reactor. Because such changes can be a source of deposition variations under nominally identical source temperature and carrier flow rates, they must be recognized and understood. Hence, we also studied the dehydration and phase-change properties of $Zn(acac)_2$ as a function of heating rate and temperature history using thermogravimetric analysis with mass spectrometry (TGA-MS), Fourier transform IR spectroscopy (FTIR), and X-ray diffraction (XRD).

Figure 1 shows a schematic of the deposition reactor. In what we will call a "standard" deposition, 100 mg of $Zn(acac)_2$ powder was placed in a boat, heated at 2°C/min to 75°C, and transported into the MOCVD chamber with 20 sccm of Ar carrier gas. Delivery lines and chamber walls were heated to prevent precursor condensation on the walls. The gas inlet tube (4 mm i.d.) was 20 mm above the substrate and produced a stagnation point flow across the substrate. Oxygen gas was introduced through a different inlet at a flow rate of 20 sccm. The total pressure was kept at 2.2 Torr, and the growth durations ranged from 30 min to 24 h. The substrate temperature was maintained at 550°C. For consistency, Ar and O_2 gas flows were initiated first; then, the substrate, reactor walls, and gas lines were heated; and finally, the precursor was heated using the desired temperature-time trajectory during growth.

Results and Discussion

Substrate effects.— ZnO nanowire morphology depends sensitively on both the substrate and the growth conditions. Figure 2 shows scanning electron microscopy (SEM) images of ZnO grown on different substrates using the standard deposition conditions for 2 h. Substrates include F:SnO_2, glass, *a*- and *c*-plane sapphire, Si, and *c*-plane ZnO. Many oxide substrates, such as F:SnO_2, SiO_2, and

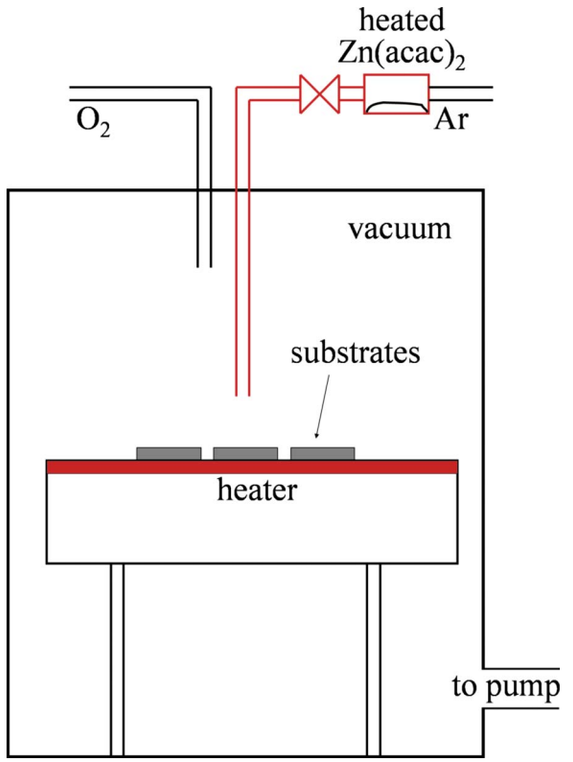

Figure 1. (Color online) Schematic of metallorganic CVD chamber. Ar carrier gas transports sublimed $Zn(acac)_2$ vapor through heated lines and into the chamber where it flows across the heated substrates in a stagnation point flow geometry. Oxygen flows into the vacuum chamber through a separate inlet.

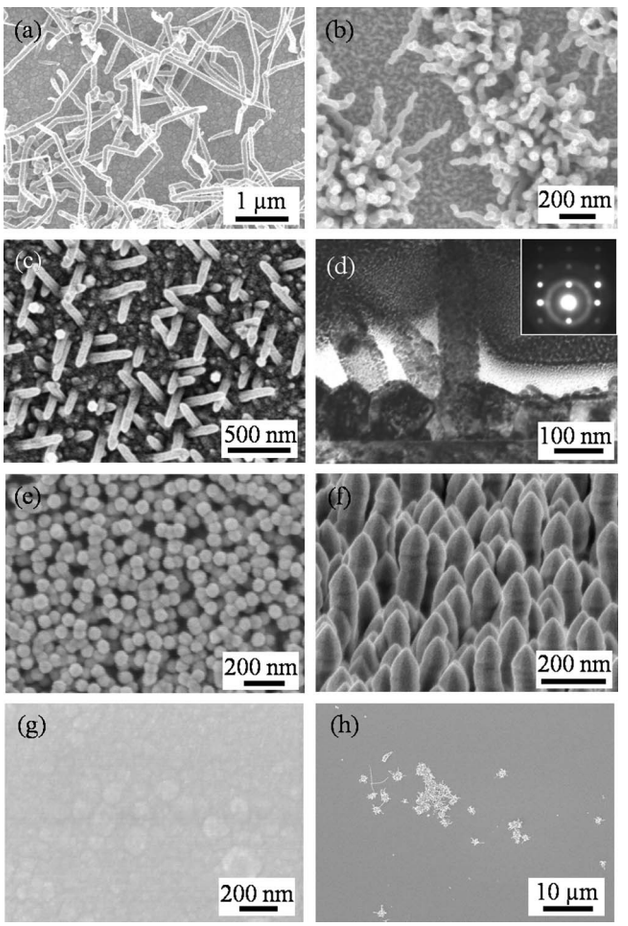

Figure 2. ZnO grown under the same growth conditions on different substrates for 2 h. Substrate temperature, total pressure, and $Zn(acac)_2$ temperature were maintained at 550°C, 2.2 Torr, and 75°C $Zn(acac)_2$, respectively. The Ar and O_2 gas flow rates were maintained at 20 sccm each. (a) Random nanowires on $F:SnO_2$, (b) random nanowires on glass, (c, d) oriented nanowires on *c*-plane sapphire, (e, f) aligned nanowires on *a*-plane sapphire, (g) polycrystalline film on *c*-plane ZnO, and (h) polycrystalline film on Si. All images are top view SEMs except that (d) is cross-sectional TEM and (f) is a glancing view SEM. The cross-sectional TEM in (d) shows the polycrystalline film whose grains serve as nucleation sites for nanowires. The inset diffraction pattern is taken with the electron beam parallel to the $[10\bar{1}0]$ zone axis of the nanowire, which grows with its *c*-axis normal to the sapphire substrate. The rings in the diffraction pattern are an artifact of a Pt-coating applied to the nanowires during sample preparation.

Al_2O_3 in Fig. 2a-f, are conducive to nanowire growth, while polycrystalline ZnO films (Fig. 2g) and Si substrates (Fig. 2h) are more prone to film growth under the conditions used in this study. Nanowires, such as those in Fig. 2a, can grow to ~5 μm in length and have fairly uniform diameters of ~100 nm. Nanowire dimensions and morphology can be varied by changing the growth conditions, as will be discussed later.

The variations in morphology from nanowires to films may arise from differences in surface and interfacial energies, different adatom diffusion rates, or different types and densities of nucleation sites for the different substrates. Nanowires grew with random orientation on polycrystalline $F:SnO_2$ and amorphous glass substrates (Fig. 2a and b) because there is no well-defined epitaxy to direct the growth. However, some crystalline substrates, such as sapphire and ZnO, have preferred epitaxial relationships with ZnO that result in growth of nanowires or films with specific orientations.

Heteroepitaxial growth on sapphire (Al_2O_3) results in either film or nanowire growth, depending on growth conditions; and the dominant epitaxial relationship depends on which plane of sapphire is being used as the substrate.[15,51,52] Although Al_2O_3 has a large lattice mismatch in some orientations, other orientations provide the necessary conditions for directional growth. For example, *c*-plane sapphire is often used as a substrate to grow ZnO films[53] and nanowires[16] with their *c*-axis oriented normal to the substrate. However, on *c*-plane sapphire, the additional $[0001]_{ZnO}\|[10\bar{1}4]_{sapphire}$ epitaxial mode can also lead to nanowire growth at a 52° angle off the substrate in any of three directions, which are separated in projection by 120°,[15] as shown in Fig. 2c and d. The inset of Fig. 2d shows an electron diffraction pattern taken from the nanowire, confirming that it is crystalline ZnO with growth along the *c*-axis. More detailed TEM electron diffraction used to determine these epitaxial relationships can be found in Ref. 15. The nanowire in Fig. 2d is growing vertically from *c*-sapphire, having nucleated from one grain of the polycrystalline seed film, as will be discussed in the next section. The presence of multiple epitaxial modes is eliminated by using *a*-plane sapphire substrates, where the $[0001]_{ZnO}\|[11\bar{2}0]_{sapphire}$, $[11\bar{2}0]_{ZnO}\|[0001]_{sapphire}$ epitaxial mode dominates while all other orientations are incommensurate.[15,52] Thus, *a*-plane sapphire substrates can be used to grow nanowires that are aligned perpendicular to the substrates as well as rotationally within the substrate plane, as shown in Fig. 2e and f. XRD pole figures confirming this epitaxial relationship can be found in Ref. 15.

Homoepitaxial growth on ZnO will likely result in film deposition because the interface creates little or no strain, and a film will have the lowest total surface energy of any morphology. Figure 2g shows a plan-view image of a ZnO film grown by MOCVD on polycrystalline, but well-oriented *c*-ZnO film that had been previ-

ously grown by plasma-enhanced CVD on a glass substrate.[54] ZnO also grew as films on Si substrates (Fig. 2h), but for different reasons. Although epitaxy between ZnO and Si has been shown to exist,[55] we did not find epitaxial growth under our growth conditions where films may have resulted simply from the lack of nucleation sites on the very flat Si surface. Occasional nanowire clusters could be found on Si, and usually correlated with sparse debris, scratches, or other imperfections on the substrate.

Nucleation and the effect of water vapor.— The diameter of the nanowires is determined primarily by the grain size of the polycrystalline films deposited on the substrate during the initial nucleation phase of the growth. A cross-sectional TEM image of ZnO nanowires grown on sapphire (Fig. 2d) shows that the nanowires nucleate and grow on top of a thin (~50 nm) polycrystalline ZnO film. This thin polycrystalline ZnO film is deposited during the initial stages of the growth. The polycrystalline film exhibits grain size on the order of 50–100 nm, which yields nanowires with similar diameters because nanowires grow directly from the *c*-face of the grains. Hence, the grain sizes in this initial film also determine the size of the nanowires that nucleate and grow from that film. Nanowires do not always grow perpendicular to the substrate because the grains are not necessarily oriented with their *c*-axis in the normal direction. Although perpendicular grains and nanowires are energetically favorable on *a*-sapphire and for some grains on *c*-sapphire because of epitaxy, there is no particular driving force for *c*-axis–oriented grains on nonepitaxial substrates. Thus, grains of the film as well as the nucleated nanowires can be oriented randomly on substrates such as glass and F:SnO_2. Furthermore, epitaxy on *c*-sapphire dictates that it is often energetically favorable to nucleate ZnO grains and nanowires with their *c*-axis not aligned normal to the substrate, as evident with the two nanowires on the left-hand side of Fig. 2d. In the case of the polycrystalline ZnO substrate, nanowires do not grow at all. It is likely that the initial stage of MOCVD uniformly coats the ZnO grains of the substrate rather than forming new grains, as it does on other substrates such as sapphire. The substrate's ZnO grains are of different size and shape than those formed spontaneously during MOCVD and apparently are not conducive to nucleating nanowires.

The change in morphology, from film to nanowires, was found to be due to an inevitable transient presence of water vapor in the chamber during the initial stages of growth and will be discussed in detail below. The nanowires are single-crystal wurtzite with growth along the *c*-axis, as indicated by the diffraction pattern produced by an electron beam directed along the $[10\bar{1}0]$ zone axis and shown in the inset of Fig. 2d. It appears that many, but not all, of these grains serve as seeds for the nanowire growth. The grains have a fairly uniform size distribution that could arise from nucleation of uniform size islands with characteristic length determined by the balance of Zn flux to the surface and Zn diffusion on the surface. Figure 3a shows a plan-view SEM of many islands that have nucleated on an *a*-plane sapphire substrate. Each of the faceted islands has hexagonal structure and has the potential to nucleate a nanowire.

An often unmentioned subtlety with precursors such as $Zn(acac)_2$ is that they are hydrated and that their composition changes upon heating. Changes in $Zn(acac)_2$ composition upon heat-treatment have been studied by thermochemistry and calorimetry,[56,57] but these results have not previously been recognized as being critical to MOCVD of ZnO. Specifically, as the hydrated precursor is heated, both $Zn(acac)_2$ and H_2O vapor evolve from the precursor boat. Because water is more volatile, the precursor is rapidly dehydrated during the first ~30 min. Hydration affects the sublimation rate of $Zn(acac)_2$ and the partial pressures of both $Zn(acac)_2$ and H_2O in the growth chamber. Relative changes in the partial pressures of $Zn(acac)_2$ and H_2O during precursor heating, in turn, affect the morphology of the growing ZnO. We observed that polycrystalline film growth occurs during the first ~30 min when water evolving from the precursor is present in the MOCVD chamber. Nanowire growth follows the film-growth period after all water has been desorbed from $Zn(acac)_2$. Further sublimation of an anhydrous precursor in the absence of water vapor results in continuous growth of nanowires.

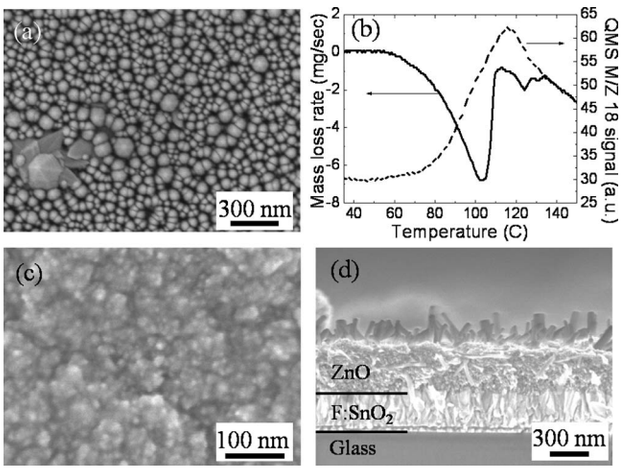

Figure 3. (a) ZnO islands on sapphire that could serve as nucleation sites for nanowire growth. (b) Mass loss rate of $Zn(acac)_2$ and mass spectrometry signal assigned to evolved water ($m/z = 18$) as a function of temperature using a 5°C/min heating rate. (c) Plan view and (d) cross-sectional SEM of ZnO films grown on F:SnO_2 using $Zn(acac)_2$ and H_2O as precursors.

Ex situ TGA-MS analysis of the precursor shows that sublimation of hydrated $Zn(acac)_2$ begins at temperatures as low as 55°C (Fig. 3b) and that H_2O evolves from the hydrated precursor during a 5°C/min ramp when the temperature is between 50 and 100°C. In situ pressure measurements and mass spectrometry confirm the ex situ TGA-MS results. Specifically, as the precursor is heated, the chamber pressure increases by ~30 mTorr due to water evolution. After the precursor is dehydrated, the chamber pressure decreases again. That the pressure rise is due to water evolution from the precursor is confirmed using in situ mass spectrometry; the pressure rise and drop corresponded to a similar rise and drop in the 18 amu peak. Ex situ TGA-MS in Fig. 3b indicates that water desorption causes the sublimation rate of the $Zn(acac)_2$ to increase by as much as a factor of four in the 70–100°C temperature range. After this initial water evolution, when the final precursor temperature is reached, the now-anhydrous precursor sublimes at a fairly constant rate for several hours. The $Zn(acac)_2$ partial pressure in the MOCVD chamber during the constant sublimation phase is typically on the order of 1 mTorr.

To confirm the effect of water on morphology, ZnO was grown using a constant background pressure of 16 mTorr H_2O in lieu of 1.1 Torr O_2. When water is introduced intentionally into the chamber, ZnO films several hundred nanometers thick with only sparse nanowire coverage on top (Fig. 3c and d) could be grown. On the basis of these observations, we propose that oxidation of $Zn(acac)_2$ with H_2O leads to film growth while oxidation by O_2 in the absence of H_2O results in nanowire growth. We surmise that because O–H bonds are more easily broken than O = O bonds, H_2O can react on all ZnO surface planes with about the same probability, whereas dissociation of O_2 can be more surface selective and yield anisotropic growth rates and, hence, nanowires. Furthermore, use of a precursor that had been previously heated to drive off water did not result in dense nanowire growth. Under our growth conditions, it appears that initial water vapor is necessary to form nucleation sites for subsequent nanowire growth. While O_2 alone can be used to grow nanowires from the polycrystalline film, it is not sufficient to cause frequent nucleation events to occur.

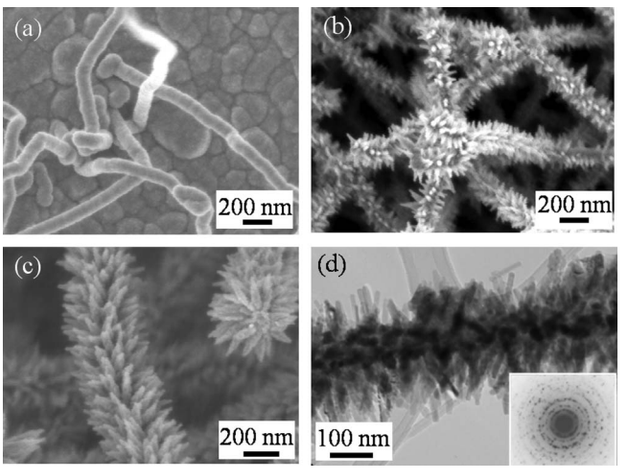

Figure 4. SEM images of ZnO nanowires (a) with smooth surfaces after 40 min of growth, (b) with small secondary nanowires after 5 h of growth, and (c) well-developed secondary nanowires after 24 h of growth. (d) TEM image of a nanowire with secondary nanowires emanating from it after 24 h of growth. Transmission electron diffraction pattern shown in the inset is taken from the ensemble of nanowires. The rings of spots indicate that the ensemble is a collection of many crystalline nanowires.

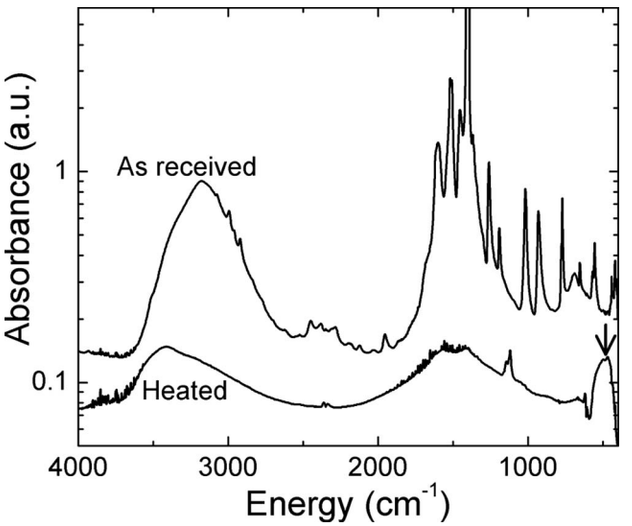

Figure 5. FTIR absorbance of precursor before and after heating at 75°C for 24 h. Absorptions assigned to acetylacetonate ligands decrease, position of OH shifts, and Zn–O vibration appears after heating. The Zn–O vibration at 450 cm^{-1} is marked with an arrow. Spectra are offset for clarity.

Effect of growth time.— ZnO nanowire morphology also depends on growth time. During the first few hours of growth, ZnO nanowires nucleate and grow to several microns in length from sites on the polycrystalline film. The nanowires grown for up to 3 h tend to have smooth surfaces and are ~100 nm diameter, as shown in Fig. 4a. TEM and electron diffraction (Fig. 2d) show that the primary nanowires are locally single crystals. The nanowires kink and curl as they grow, possibly due to strain or twinning in the lattice, and may be polycrystalline over their entire length. After a few hours, axial growth of the nanowires slows but secondary nanowires nucleate and grow from the primary nanowire backbone. For example, Fig. 4b shows branched nanowires obtained after 5 h of growth. These branched nanowires grow longer and denser over time; after 24 h, the secondary nanowires are ~20 nm diameter and ~100 nm in length (Fig. 4c). The size and density of the secondary nanowires significantly increase the surface area of the nanowires, making them potentially useful in applications such as dye sensitized solar cells and sensors.[1,3] The electron diffraction pattern shown in the inset of Fig. 4d was taken from an ensemble of nanowires and shows rings of spots that appear because the electron beam was incident on multiple crystals that have the same lattice constants but are randomly oriented. Although the primary nanowire and each of the secondary nanowires are crystalline, there are grain boundaries at the interfaces between them. Thus, the whole structure appears polycrystalline in electron diffraction. However, because only a single grain boundary exists at the branching point, this microstructure is still suitable for applications such as dye-sensitized solar cells, where photogenerated electrons must be transported from the point of generation to an electrode while crossing as few grain boundaries as possible. The high density of secondary nanowires makes it difficult to determine if the secondary nanowires in Fig. 4c have any orientational relationship to the original nanowire, although thicker nanowires discussed later (Fig. 7d) indicate that the secondary nanowires may grow in preferred directions from the primary nanowire backbone. In fact, Gao and Wang have shown epitaxial growth of secondary nanowires using two-step thermal evaporation.[25]

The changing morphology of the ZnO from film to nanowires to secondary nanowires coincides with the precursor changing from hydrated $Zn(acac)_2$ to anhydrous $Zn(acac)_2$ to ZnO. Decomposition of the $Zn(acac)_2$ within the heating cell during ZnO nanowire growth was confirmed using ex situ transmission FTIR by comparing as-received and heat-treated $Zn(acac)_2$. Each powder was mixed with KBr pellets, pressed into a thin disk, and placed in the path of the IR beam. FTIR spectra for the as-received $Zn(acac)_2$ and $Zn(acac)_2$ that had been heated at 75°C for 24 h (to simulate a long growth experiment) are shown in Fig. 5. The as-received powder shows many absorption peaks between 800 and 1800 cm^{-1} that can be assigned to the vibrational modes of the acetatylacetonate ligand. For example, the intense peaks at 1392 and 1593 cm^{-1} are assigned to CH_3 deformation and C = O stretching modes, respectively.[58] The broad absorption feature in the 2700–3600 cm^{-1} range is due to water molecules hydrating $Zn(acac)_2$. The powder that underwent heat-treatment shows three major differences from the as-received powder. First, the acetatylacetonate absorptions are significantly decreased (note logarithmic scale of Fig. 5). Second, the OH stretching peak shifts to higher energies typical of isolated and associated Zn–OH species. Third, a new peak emerges at 450 cm^{-1} that is assigned to the Zn–O stretching mode in ZnO.[58] Thus, over the course of a long nanowire growth experiment, the identity of the heated precursor changes from $Zn(acac)_2$ hydrate to anhydrous $Zn(acac)_2$ to ZnO. The changing composition of the precursor was also confirmed by XRD 2θ scans. XRD of the as-received powder shows crystalline $Zn(acac)_2$. However, XRD of precursor that had been heat-treated for 24 h at 75°C shows that it has completely changed to ZnO (data not shown).

The changing composition of the precursor affects ZnO growth rate and morphology because ZnO has much lower vapor pressure than $Zn(acac)_2$, drastically reducing the concentration of Zn delivered to the reaction chamber. The mechanisms and morphologies of ZnO growth from molecular ZnO or a partially decomposed precursor are also likely quite different from growth from $Zn(acac)_2$ due to different decomposition and crystallization kinetics on the nanowire surfaces.

After ~24 h of growth, the precursor is depleted and all growth slows down and eventually stops. The precursor can be replenished and growth can be continued on substrates that already have nanowires. Here, we call nanowires grown on a substrate that already has nanowires "second generation." During the growth of a second generation of nanowires, the secondary nanowires act as nucleation sites. Upon replacing the precursor and increasing the temperature back to 75°C, the second generation of nanowires grows from the

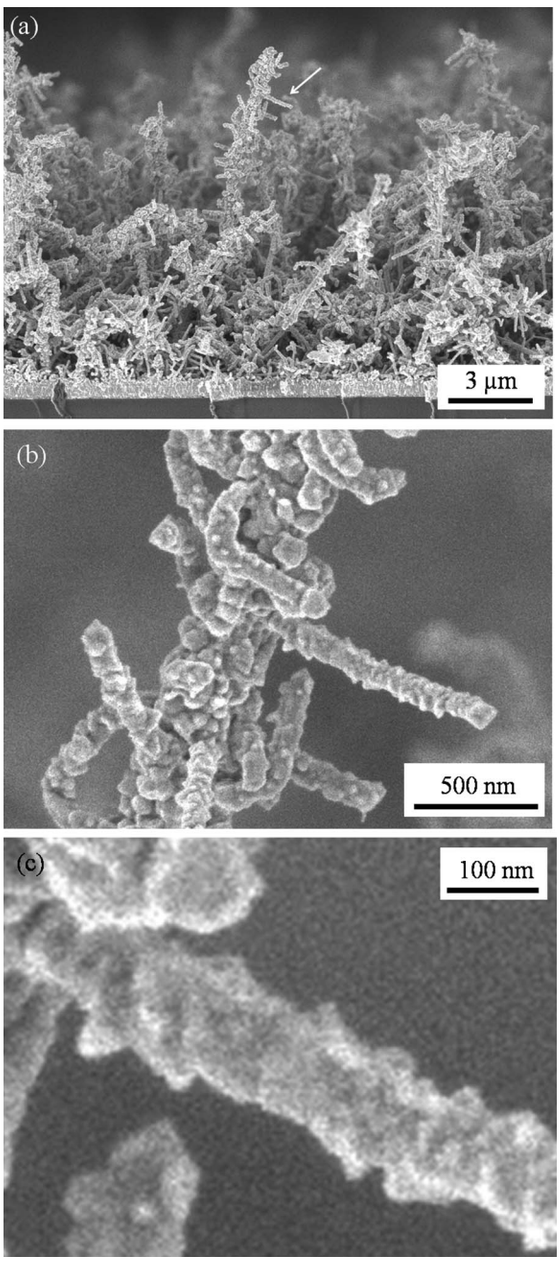

Figure 6. Cross-sectional SEM images of branched ZnO nanowires after two 24 h growth cycles. (b) and (c) show the area marked with an arrow in (a) at increasing magnification. During the second cycle, nanowires nucleate and grow from the branch points on the first generation of nanowires (see Fig. 4b-d) and from the substrate.

secondary nanowires of the first generation. Figure 6 shows the resulting dendrite-like branched structure of second-generation nanowires. The cross-sectional SEM of second generation nanowires in Fig. 6b shows the branched structure as well as the connectivity of the branching nanowires to the substrate via the primary nanowires. After growing for 24 h, the second-generation nanowires will then have secondary nanowires that can serve as nucleation sites for a third generation. The growth can be continued for additional generations, if desired, although film growth during the initial heating of the precursor can begin to fill some of the porous structure. Because this branching occurs as a result of changes to the precursor only, it can be seen for all substrates that are conducive to nanowire growth.

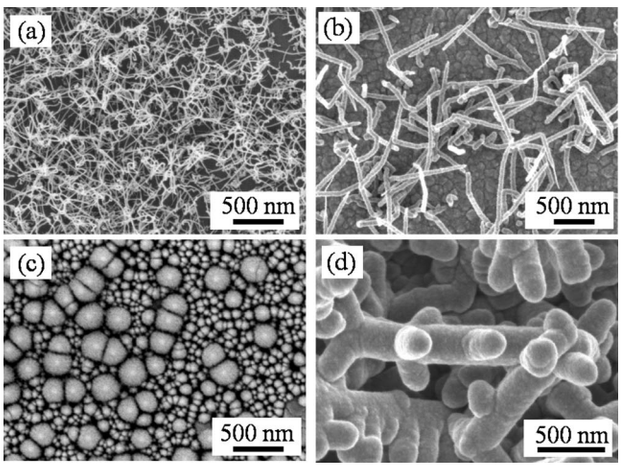

Figure 7. SEM images of ZnO growth on sapphire at chamber pressures of (a) 0.2, (b) 2.2, and (c) 10 Torr. (d) ZnO nanowires grown by loading the boat with 300 mg instead of 100 g of $Zn(acac)_2$; increased partial pressure of $Zn(acac)_2$ results in larger nanowire diameters. Secondary growth in (d) is due to longer growth time as described in Fig. 4.

Effect of pressure and temperature on morphology.— In addition to substrate, presence of water vapor, and composition of precursor, ZnO morphology is also strongly affected by the growth conditions, such as the partial pressure of the precursors and the substrate temperature. Pressure and temperature affect both the nucleation and the continuous growth phases; thus, ZnO growth was examined after 2 h to investigate how these variables influence the morphology. The partial pressure of $Zn(acac)_2$ in the growth chamber is determined by the amount and the surface area of precursor powder loaded into the delivery boat, the precursor temperature, the carrier gas flow rate, and the chamber pumping speed. Because partial pressure of $Zn(acac)_2$ depends on many factors, we found it convenient to adjust the total pressure by varying the pumping speed while keeping the ratio of gas flow rates constant. To change the partial pressure of $Zn(acac)_2$, we loaded different predetermined weights of precursor into the boat (e.g., from 100 to 300 mg). Figures 7a-c show the dependence of morphology on the total chamber pressure. At low pressures $\sim$80 mTorr, Fig. 7a, nanowires were thinner with more kinks and bends. At higher pressures $\sim$20 Torr, Fig. 7c, nanowire growth did not occur at all, although ZnO islands, many of which had diameters of $>$300 nm, did form on the substrate. At the intermediate pressure of 2.2 Torr, nanowires grew to 5 μm long with 100 nm diam and few kinks (Fig. 7b). When the precursor loading was changed from 100 to 300 mg while keeping the total pressure constant, nanowire diameter increased from $\sim$100 to $\sim$ 300 nm, as shown in Fig. 7d. Thus, ZnO nanowire diameter increases with increasing $Zn(acac)_2$ partial pressure. The nanowires in Fig. 7d are branched as a result of longer growth time, as discussed previously. Increasing the precursor loading from 100 to 300 mg increased the $Zn(acac)_2$ partial pressure from $\sim$1 to 3 mTorr, as measured by a pressure gauge attached to the growth chamber.

Morphology also depends on temperature and only a narrow window of substrate temperatures, $\sim$500 to 600°C, is conducive to nanowire growth. Figure 8 shows the effect of substrate temperature on the nanowire morphology. The nanowire structures were present at 600°C (Fig. 8a), but the nanowire cross sections were not nearly as well faceted as those at 550°C. Figure 8b shows well-faceted hexagonal nanowires grown at 550°C on *a*-sapphire. At 500°C (Fig. 8c), there was a much wider distribution of shapes of the structures and only a few nanowires were present. The nanowire morphology likely depends on temperature through its influence on competition between activated processes such as the growth kinetics on different

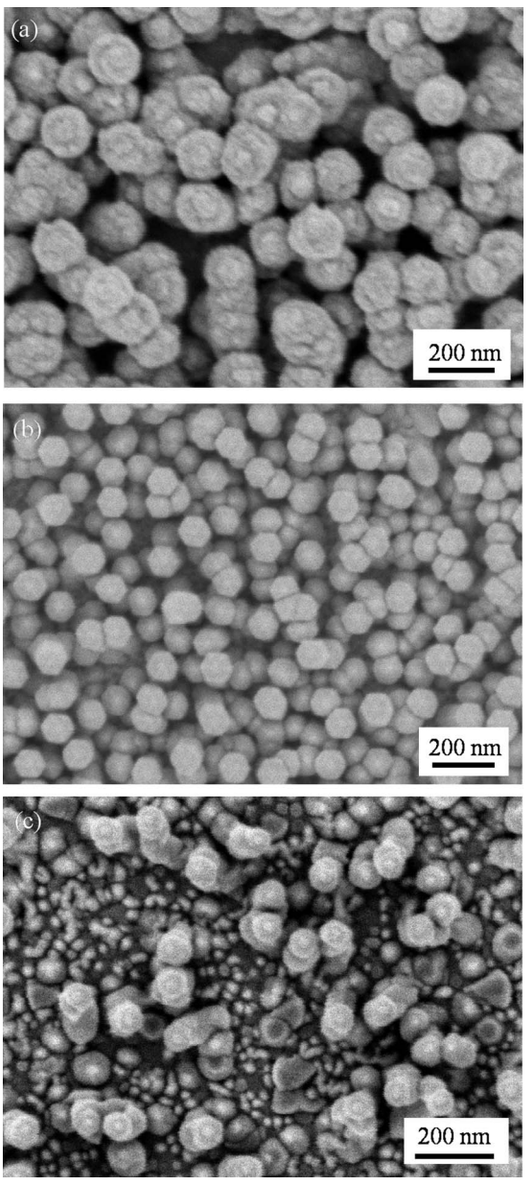

Figure 8. ZnO grown on sapphire at (a) 600, (b) 550, and (c) 500°C, demonstrating the narrow temperature window in which well-defined nanowires can be grown. All scale bars are 200 nm.

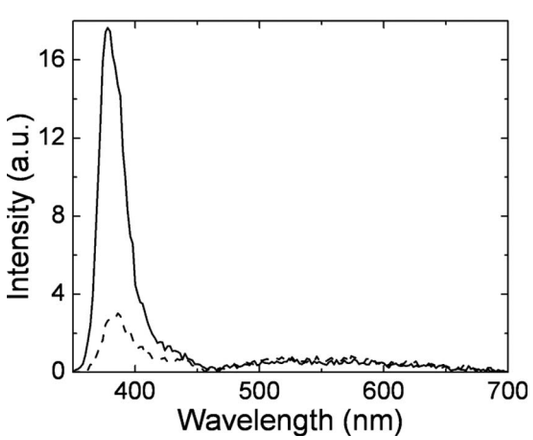

Figure 9. Room temperature PL spectra of ZnO nanowires before (dotted) and after (solid) H_2 plasma treatment.

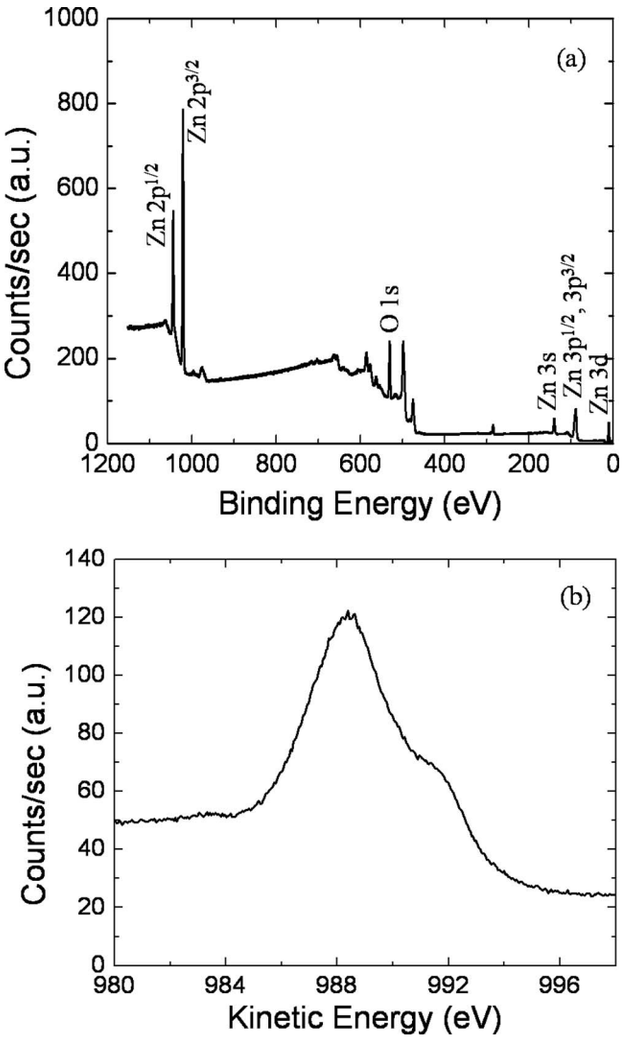

Figure 10. (a) XPS survey spectrum of ZnO nanowires using Al Kα excitation source, with peaks labeled according to Ref. 60. (b) Auger spectrum of Zn LMM peak demonstrating the major presence of ZnO (988.4 eV) with traces of Zn (992.0 eV).

surfaces and the diffusion rates of adatoms. Growth conditions outside the narrow window of substrate temperature and $Zn(acac)_2$ pressure presented here resulted in growth of ZnO films or no ZnO deposition at all.

Characterization of ZnO bulk and surface properties.— ZnO nanowires were further characterized using PL and XPS. Room-temperature PL performed using 325 nm excitation shows band-edge emission at 380 nm (Fig. 9), indicating the good crystallinity of the wurtzite structure. This UV peak was enhanced significantly by treating the nanowires in H_2 plasma. The H_2 plasma may act by healing defects, passivating dangling bonds, or removing residual carbon. There is also a small broad emission centered around 510 nm present for both plasma-treated and as-grown samples. This green emission is typically attributed to deep-level defects, such as singly ionized oxygen vacancies, and did not change with H_2 plasma treatment.[59]

The surface structure of the ZnO nanowires was investigated by XPS. Data were taken with Al Kα excitation having a total energy 1486.6 eV using a Kratos Axis Ultra instrument equipped for XPS and Auger spectroscopy. Figure 10a shows an XPS survey spectrum of nanowires grown by MOCVD with the strongest line at a binding

energy of 1021.6 eV, assigned to Zn $2p^{3/2}$.[60] Other lines correspond to other transitions in Zn or O and are labeled in Fig. 10a according to assignments made by Langer and Vesely.[60] No significant levels of any impurities were detected. Figure 10b shows an Auger spectrum with the peak centered at kinetic energy of 988.4 eV assigned to the Zn LMM transition in ZnO.[61] This transition was used instead of transitions with higher intensities because of the large difference in peak location between Zn and ZnO. The small shoulder centered at 992.0 eV is assigned to the Zn LMM transition in Zn.[61] The peak shape and position show that the material is predominantly ZnO, but may have small Zn domains present.

Conclusions

ZnO nanowires were grown on a variety of oxide substrates from $Zn(acac)_2$ and O_2. Morphology of the nanowires depends on the temperature history of the precursor, growth time, substrate temperature, pressure, and substrate material. Nanowires nucleate from a thin ZnO film that grows as a result of the water initially adsorbed to the hydrated precursor. The ZnO nanowires are crystalline with few impurities. Nanowires with a branched structure can be grown by extending the growth time, greatly increasing the nanowire surface area, and enabling the use of nanowires in applications such as dye-sensitized solar cells and sensors.

Acknowledgments

This work was carried out in the Department of Chemical Engineering at the University of California Santa Barbara. It was supported by the University of California Energy Institute's Energy Science and Technology Program and made use of MRL Central Facilities supported by the MRSEC Program of the National Science Foundation under grant no. DMR00-80034. J.B.B. was supported by a National Science Foundation Graduate Research Fellowship.

Drexel University assisted in meeting the publication costs of this article.

References

1. J. B. Baxter and E. S. Aydil, *Appl. Phys. Lett.*, **86**, 053114 (2005).
2. M. Law, L. E. Greene, J. C. Johnson, R. Saykally, and P. D. Yang, *Nature Mater.*, **4**, 455 (2005).
3. J. B. Baxter and E. S. Aydil, *Sol. Energy Mater. Sol. Cells*, **90**, 607 (2006).
4. J. B. Baxter, A. M. Walker, K. van Ommering, and E. S. Aydil, *Nanotechnology*, **17**, S304 (2006).
5. Q. Wan, Q. H. Li, Y. J. Chen, T. H. Wang, X. L. He, J. P. Li, and C. L. Lin, *Appl. Phys. Lett.*, **84**, 3654 (2004).
6. H. T. Wang, B. S. Kang, F. Ren, L. C. Tien, P. W. Sadik, D. P. Norton, S. J. Pearton, and J. Lin, *Appl. Phys. Lett.*, **86**, 243503 (2005).
7. Y. S. Zhang, K. Yu, D. S. Jiang, Z. Q. Zhu, H. R. Geng, and L. Q. Luo, *Appl. Surf. Sci.*, **242**, 212 (2005).
8. M. H. Huang, S. Mao, H. Feick, H. Q. Yan, Y. Y. Wu, H. Kind, E. Weber, R. Russo, and P. D. Yang, *Science*, **292**, 1897 (2001).
9. J. H. Choy, E. S. Jang, J. H. Won, J. H. Chung, D. J. Jang, and Y. W. Kim, *Adv. Mater. (Weinheim, Ger.)*, **15**, 1911 (2003).
10. C. J. Lee, T. J. Lee, S. C. Lyu, Y. Zhang, H. Ruh, and H. J. Lee, *Appl. Phys. Lett.*, **81**, 3648 (2002).
11. Y. W. Zhu, H. Z. Zhang, X. C. Sun, S. Q. Feng, J. Xu, Q. Zhao, B. Xiang, R. M. Wang, and D. P. Yu, *Appl. Phys. Lett.*, **83**, 144 (2003).
12. Y. K. Tseng, C. J. Huang, H. M. Cheng, I. N. Lin, K. S. Liu, and I. C. Chen, *Adv. Funct. Mater.*, **13**, 811 (2003).
13. J. J. Wu and S. C. Liu, *J. Phys. Chem. B*, **106**, 9546 (2002).
14. J. J. Wu and S. C. Liu, *Adv. Mater. (Weinheim, Ger.)*, **14**, 215 (2002).
15. J. B. Baxter and E. S. Aydil, *J. Cryst. Growth*, **274**, 407 (2005).
16. W. I. Park, D. H. Kim, S. W. Jung, and G. C. Yi, *Appl. Phys. Lett.*, **80**, 4232 (2002).
17. A. R. Kaul, O. Y. Gorbenko, A. N. Botev, and L. I. Burova, *Superlattices Microstruct.*, **38**, 272 (2005).
18. W. Lee, M. C. Jeong, and J. M. Myoung, *Acta Mater.*, **52**, 3949 (2004).
19. M. H. Huang, Y. Y. Wu, H. Feick, N. Tran, E. Weber, and P. D. Yang, *Adv. Mater. (Weinheim, Ger.)*, **13**, 113 (2001).
20. T. Ghoshal, S. Biswas, S. Kar, A. Dev, S. Chakrabarti, and S. Chaudhuri, *Nanotechnology*, **19**, 065606 (2008).
21. F. Li, Z. Li, and F. J. Jin, *Physica B*, **403**, 664 (2008).
22. P. Prete, N. Lovergine, and L. Tapfer, *Appl. Phys. A: Mater. Sci. Process.*, **88**, 21 (2007).
23. W. W. Wang, G. M. Zhang, L. G. Yu, X. Bai, Z. X. Zhang, and X. Y. Zhao, *Physica E (Amsterdam)*, **36**, 86 (2007).
24. Z. R. Dai, Z. W. Pan, and Z. L. Wang, *Adv. Funct. Mater.*, **13**, 9 (2003).
25. P. X. Gao and Z. L. Wang, *Appl. Phys. Lett.*, **84**, 2883 (2004).
26. X. D. Wang, C. J. Summers, and Z. L. Wang, *Nano Lett.*, **4**, 423 (2004).
27. M. Kirkham, X. D. Wang, Z. L. Wang, and R. L. Snyder, *Nanotechnology*, **18**, 365304 (2007).
28. Z. L. Wang, *J. Nanosci. Nanotechnol.*, **8**, 27 (2008).
29. J. B. Cui and U. J. Gibson, *Appl. Phys. Lett.*, **87**, 133108 (2005).
30. Y. Li, G. W. Meng, L. D. Zhang, and F. Phillipp, *Appl. Phys. Lett.*, **76**, 2011 (2000).
31. J. Elias, R. Tena-Zaera, and C. Levy-Clement, *J. Phys. Chem. C*, **112**, 5736 (2008).
32. Y. F. Gao, M. Nagai, T. C. Chang, and J. J. Shyue, *Cryst. Growth Des.*, **7**, 2467 (2007).
33. R. Konenkamp, R. C. Word, M. Dosmailov, J. Meiss, and A. Nadarajah, *J. Appl. Phys.*, **102**, 056103 (2007).
34. L. Li, S. S. Pan, X. C. Dou, Y. G. Zhu, X. H. Huang, Y. W. Yang, G. H. Li, and L. D. Zhang, *J. Phys. Chem. C*, **111**, 7288 (2007).
35. L. Vayssieres, *Adv. Mater. (Weinheim, Ger.)*, **15**, 464 (2003).
36. L. E. Greene, M. Law, J. Goldberger, F. Kim, J. C. Johnson, Y. F. Zhang, R. J. Saykally, and P. D. Yang, *Angew. Chem., Int. Ed.*, **42**, 3031 (2003).
37. C. H. Ku and J. J. Wu, *J. Phys. Chem. B*, **110**, 12981 (2006).
38. R. B. Peterson, C. L. Fields, and B. A. Gregg, *Langmuir*, **20**, 5114 (2004).
39. S. Y. Li, C. Y. Lee, and T. Y. Tseng, *J. Cryst. Growth*, **247**, 357 (2003).
40. R. J. H. Morris, M. G. Dowsett, S. H. Dalal, D. L. Baptista, K. B. K. Teo, and W. I. Milne, *Surf. Interface Anal.*, **39**, 898 (2007).
41. P. D. Yang, H. Q. Yan, S. Mao, R. Russo, J. Johnson, R. Saykally, N. Morris, J. Pham, R. R. He, and H. J. Choi, *Adv. Funct. Mater.*, **12**, 323 (2002).
42. L. E. Greene, M. Law, D. H. Tan, M. Montano, J. Goldberger, G. Somorjai, and P. D. Yang, *Nano Lett.*, **5**, 1231 (2005).
43. J. B. Baxter and C. A. Schmuttenmaer, *J. Phys. Chem. B*, **110**, 25229 (2006).
44. M. Wang, X. L. Cao, H. X. Wang, G. M. Hua, Y. X. Lin, and L. D. Zhang, *Chem. Lett.*, **35**, 1234 (2006).
45. M. Z. Wu, L. Z. Yao, W. L. Cai, G. W. Jiang, X. G. Li, and Z. Yao, *J. Mater. Sci. Technol.*, **20**, 11 (2004).
46. H. Sato, T. Minami, T. Miyata, S. Takata, and M. Ishii, *Thin Solid Films*, **246**, 65 (1994).
47. K. Haga, T. Shishido, K. Nakajima, and T. Matsunaga, *Surf. Rev. Lett.*, **14**, 783 (2007).
48. K. Haga, T. Suzuki, Y. Kashiwaba, H. Watanabe, B. P. Zhang, and Y. Segawa, *Thin Solid Films*, **433**, 131 (2003).
49. Y. Kashiwaba, F. Katahira, K. Haga, T. Sekiguchi, and H. Watanabe, *J. Cryst. Growth*, **221**, 431 (2000).
50. H. Saitoh, M. Satoh, N. Tanaka, Y. Ueda, and S. Ohshio, *Jpn. J. Appl. Phys., Part 1*, **38**, 6873 (1999).
51. H. T. Ng, B. Chen, J. Li, J. E. Han, M. Meyyappan, J. Wu, S. X. Li, and E. E. Haller, *Appl. Phys. Lett.*, **82**, 2023 (2003).
52. P. Fons, K. Iwata, A. Yamada, K. Matsubara, S. Niki, K. Nakahara, T. Tanabe, and H. Takasu, *Appl. Phys. Lett.*, **77**, 1801 (2000).
53. Y. F. Chen, D. M. Bagnall, H. J. Koh, K. T. Park, K. Hiraga, Z. Q. Zhu, and T. Yao, *J. Appl. Phys.*, **84**, 3912 (1998).
54. T. M. Barnes, S. Hand, J. Leaf, and C. A. Wolden, *J. Vac. Sci. Technol. A*, **22**, 2118 (2004).
55. R. C. Wang, C. P. Liu, and J. L. Huang, *Appl. Phys. Lett.*, **89**, 173121 (2006).
56. T. Arii and A. Kishi, *J. Therm Anal. Calorim.*, **83**, 253 (2006).
57. G. A. M. Hussien, *Thermochim. Acta*, **186**, 187 (1991).
58. K. Nakamoto, A. E. Martell, and P. J. McCarthy, *J. Am. Chem. Soc.*, **83**, 1272 (1961).
59. K. Vanheusden, W. L. Warren, C. H. Seager, D. R. Tallant, J. A. Voigt, and B. E. Gnade, *J. Appl. Phys.*, **79**, 7983 (1996).
60. D. W. Langer and C. J. Vesely, *Phys. Rev. B*, **2**, 4885 (1970).
61. G. Deroubaix and P. Marcus, *Surf. Interface Anal.*, **18**, 39 (1992).